

Article | Received 25 October 2023; Accepted 18 March 2024; Published 12 April 2024
<https://doi.org/10.55092/bm20240002>

Supplementary information

Mimicking 3D bone microenvironment using a hybrid hydrogel-nanocomposite scaffold and human adipose-derived stem cells for bone differentiation and vascularization

Amel Ibrahim^{1,2,†,*}, Oliver FW Gardner¹, Naira Rodriguez-Florez^{1,2,‡}, John C Hutchinson³, Alexander Seifalian⁴, Daniel Thomas-Vazque⁵, Neil J Sebire^{1,3} David Dunaway^{1,6}, Neil W Bulstrode^{1,2}, Patrizia Ferretti^{1,†,*}

¹ Stem Cells and Regenerative Medicine Section, UCL Great Ormond Street Institute of Child Health, London, UK

² Department of Plastic Surgery, Great Ormond Street Hospital for Children NHS Foundation Trust, London, UK

³ Department of Histopathology, Great Ormond Street Hospital for Children, NHS Foundation Trust, London, UK

⁴ Nanotechnology and Regenerative Medicine Commercialization Centre (Ltd), The London Bioscience Innovation Center, London, UK

⁵ Johnson Space Center, NASA Pkwy, Houston, Texas, USA

⁶ Craniofacial Group - FaceValue UCL Great Ormond Street Institute of Child Health and Great Ormond Street Hospital for Children, London, UK

† Current affiliation: Bioworkshop, New York, USA

‡ Current affiliation: Universidad de Navarra, TECNUN Escuela de Ingenieros, San Sebastian, Spain and IKERBASQUE, Basque Foundation for Science, Bilbao, Spain

* Correspondence authors: Amel Ibrahim and Patrizia Ferretti;
E-mails: amel.ibrahim.11@alumni.ucl.ac.uk; p.ferretti@ucl.ac.uk.



Copyright©2024 by the authors. Published by ELSP. This work is licensed under Creative Commons Attribution 4.0 International License, which permits unrestricted use, distribution, and reproduction in any medium provided the original work is properly cited.

Table S1. Antibodies and fluorescent dye used in the study.

Primary antibodies	Species	Dilution	Source
Vimentin	Mouse	1:100	DAKO
Osteopontin	Rabbit	1:100	Abcam
Lamin A/C	Mouse	1:100	Abcam
Laminin	Mouse	1:100	Hybridoma bank
Nestin	Rabbit	1:100	Millipore
Collagen 1	Rabbit	1:100	NOVUS
Von Willebrand Factor	Rabbit	1:5000	DAKO
Human nuclear antigen	Mouse	1:100	Millipore
Secondary Antibodies/ Nuclear staining	Species	Dilution	Source
Hoechst 33258	-	1:400	Thermo Fisher Scientific
Anti-Mouse IgG Alexa Fluor 594	Goat	1:400	Invitrogen
Anti-Rabbit IgG Alexa Fluor 488	Goat	1:400	Invitrogen

Table S2. Measurements of uniaxial compression of POSS-PCL scaffolds.

	Control (n=5)	UV (n=3)	ETOH (n=3)	Decon (n=3)	Autoclave (n=2)
E (GPa)	0.91 ± 0.01	0.98 ± 0.01	0.99 ± 0.003	0.96 ± 0.01	0.96
Yield strain, ϵ (mm/mm)	2.16 ± 0.55	1.03 ± 0.29**	0.65 ± 0.11****	1.20 ± 0.34*	0.79**
Yield stress, σ (MPa)	0.29 ± 0.15	0.26 ± 0.12	0.14 ± 0.04	0.12 ± 0.02	0.06
U_{el}^{Max} (kJ/m ³)	0.27 ± 0.19	0.10 ± 0.04	0.05 ± 0.02	0.07 ± 0.02	0.02

UV: ultraviolet light, ETOH; 70% ethanol, Decon: Decon 90; statistical significance; *p < 0.05; **p < 0.01; ***p < 0.001; ****p < 0.0001.

Table S3. Sequences of primers used for RT-qPCR.

Gene	Forward (FW) & Reverse (REV) Primers (5'-3')
GAPDH	FW TGATGACATCAAGAAGGTGGTGAAG REV TCCTTGGAGGCCATGTGGGCCAT
OSC	FW ACACTCCTCGCCCTATTG REV GATGTGGTCAGCCAACCTC
ALP	FW CACGGGCACCATGAAGGAAAAG REV TGGCGCAGGGGCACAGGAGACT

ALP; Alkaline Phosphatase, GAPDH; Glyceraldehyde-3-Phosphate Dehydrogenase, OSC; Osteocalcin.

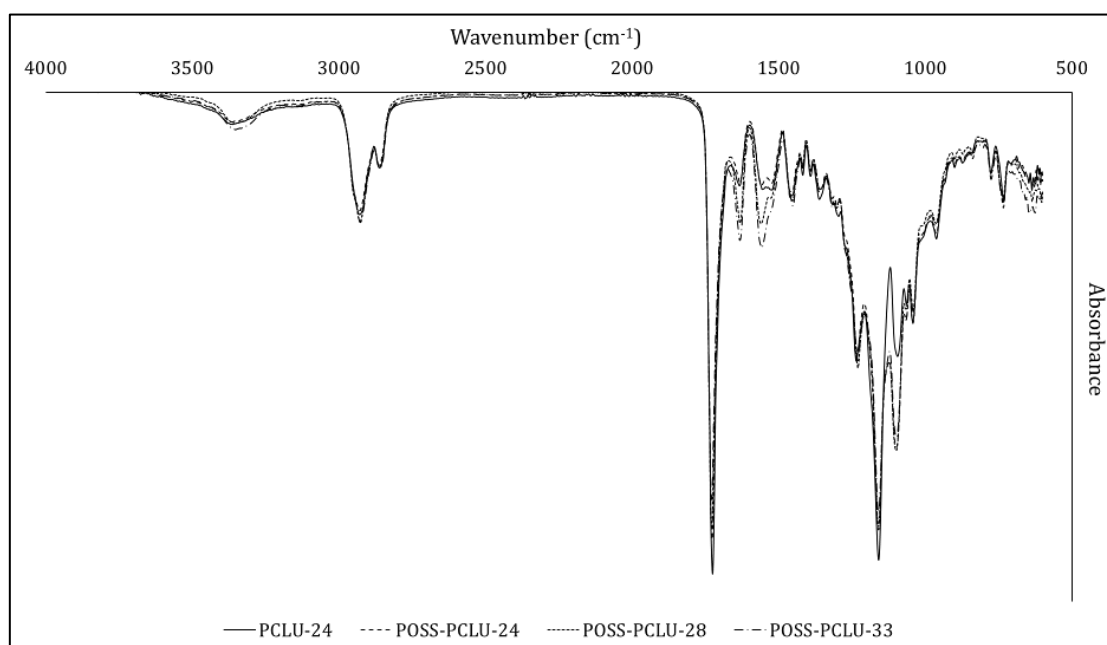


Figure S1. Overlaid attenuated total reflectance (ATR)-Fourier transform infrared (FTIR) spectrograph of cast PCLU-24, POSS-PCLU-24, POSS-PCLU-28 and POSS-PCLU-33 samples. Both urethane and urea groups at 1551 cm^{-1} and 1633 cm^{-1} , respectively, predictably increase with increasing hard segment content. The peak at 1094 cm^{-1} represents the Si-O-Si bonds and is not present for PCLU-24 which lacks POSS nanoparticles. Keys: PCLU-24; Poly(ϵ -caprolactone urea)urethane is without the POSS. POSS-PCLU-24, POSS-PCLU-28 and POSS-PCLU-33 have varying the amount of dicyclohexylmethane diisocyanate to obtain polyurethanes of 24 %, 28 %, and 33 % hard segment, all with POSS nanoparticles.

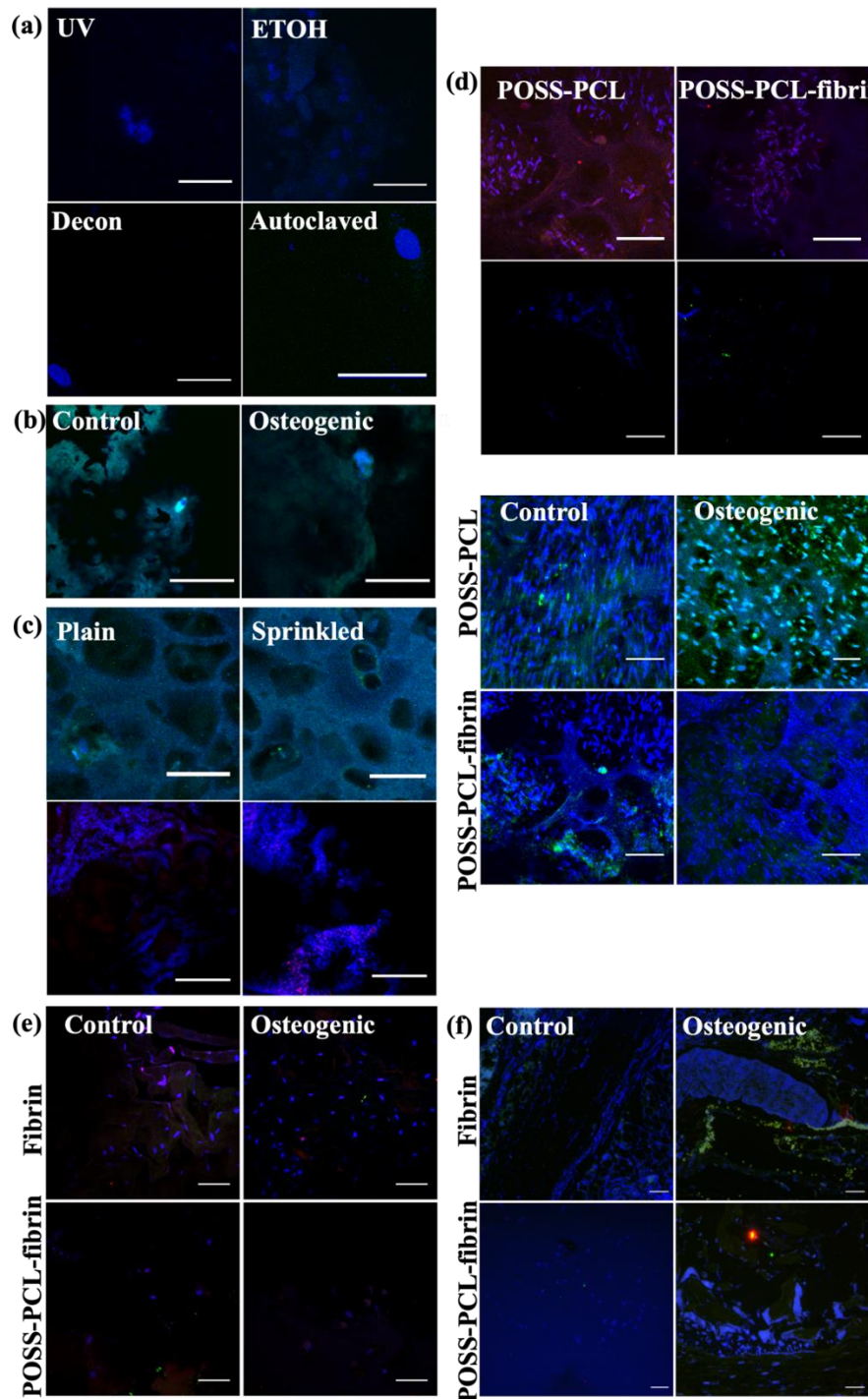


Figure S2. Immunostaining negative controls (primary antibody omitted). **a)** Figure 2E negative controls labelled with 488. **b)** Figure 3 negative controls for (d) (top row) labelled with 488 and f (bottom row) labelled with 594. **c)** Figure 4 (a) (top row) labelled with 594, (b) (rows 2–3) labelled with 488 and (c) (bottom) row labelled with 488. **d)** Figure 5 (a) negative controls labelled with 488 and 594. **e)** Figure 7 negative controls labelled with 488 and 594. **f)** Supplementary Figure S1 negative controls labelled with 488. All nuclei counterstained with Hoechst. Scale bars; 50 μm (a) and 100 μm rest, negative controls; 488 (green) anti-rabbit or 594 (red) anti-mouse secondary antibody staining only.

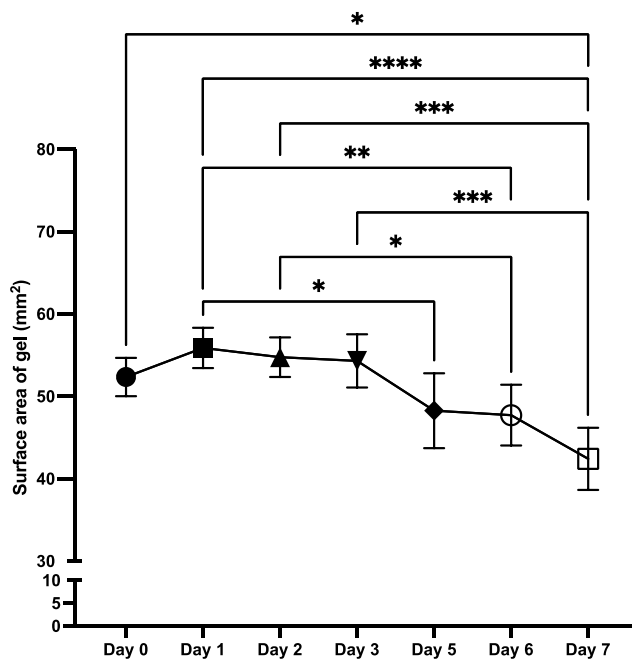
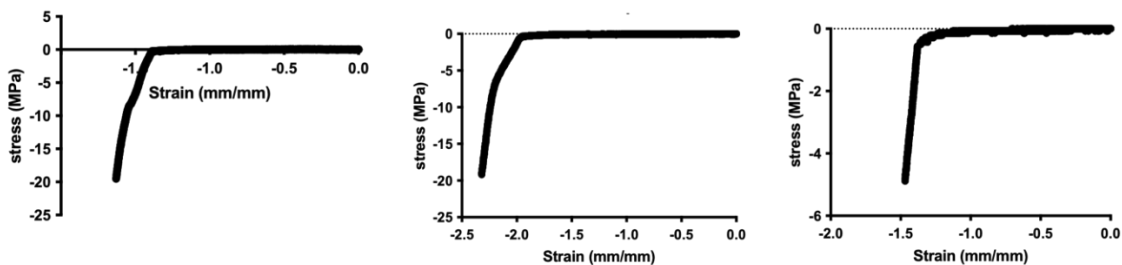


Figure S3. Contraction of hADSC seeded fibrin gels. Shrinkage of hADSC laden fibrin gels cultured *in vitro* over 7 days. Statistical significance; * $p < 0.05$, ** $p < 0.01$, *** $p < 0.001$, **** $p < 0.0001$.

Plain



Sprinkled

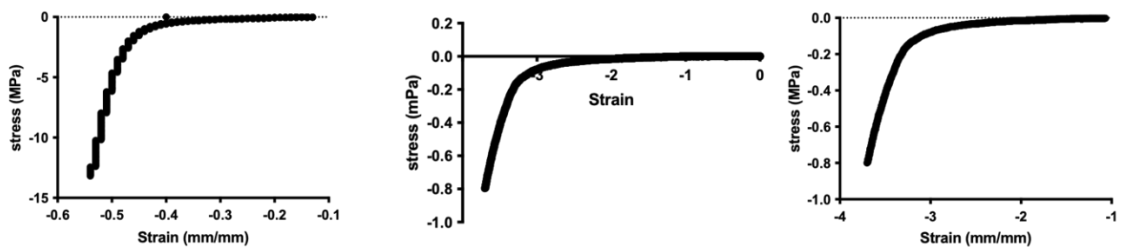


Figure S4. Stress-Strain curves of plain and sprinkled POSS-PCL to accompany Table 1.

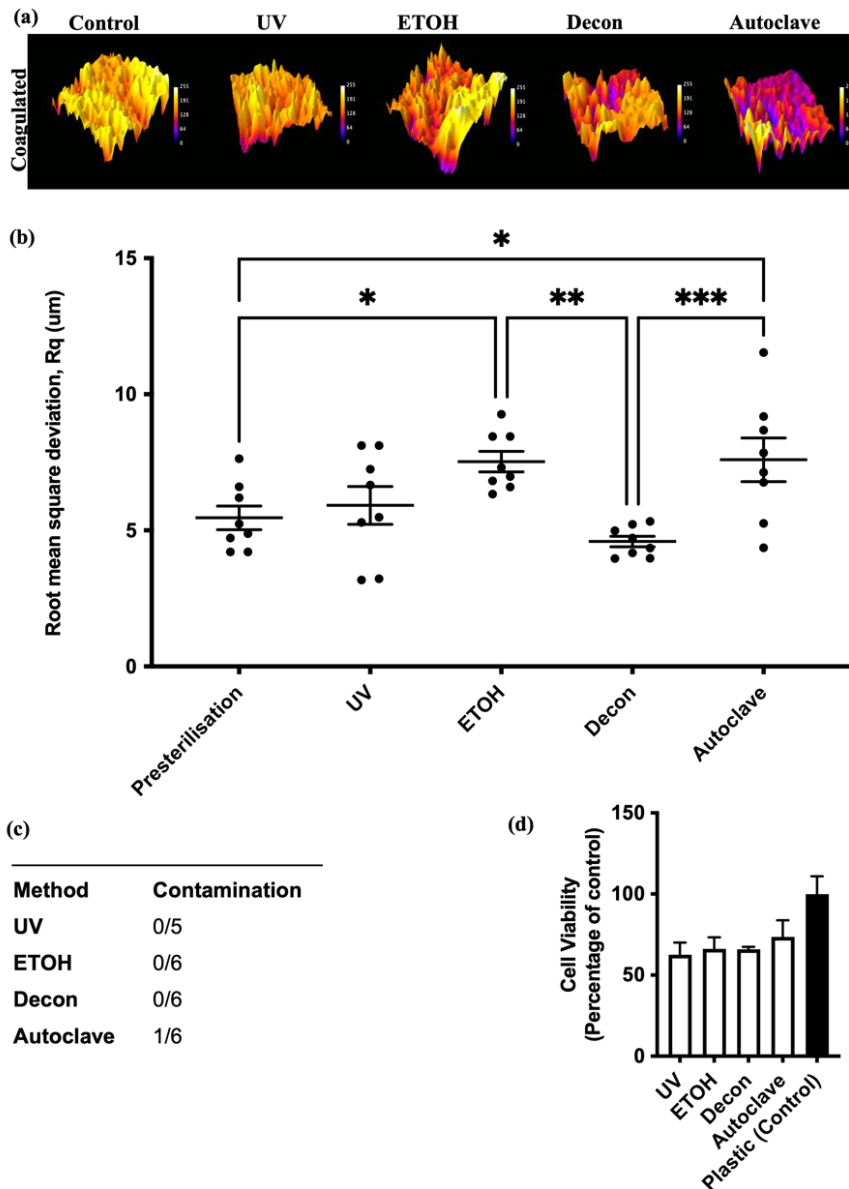


Figure S5. Effect of different sterilization techniques on POSS-PCL surface topography and hADSC behavior. **a)** Heat maps representing pixel height of POSS-PCL surfaces (yellow is highest peak and blue is lowest) to visualize topography. ETOH treatment increases roughness whereas autoclaving flattens the topography. **b)** Quantitative analysis of surface roughness. **c)** Culture medium samples assessed by light microscopy for bacterial contamination after 14 days of cell culture. **d)** hADSC quantification assessed by Resuzarin assay after 7 days in culture. Data are expressed as percentage of cells grown on plastic. UV; ultraviolet light, ETOH; 70% ethanol, Decon; Decon 90. Statistical significance; * $p < 0.05$, ** $p < 0.01$, *** $p < 0.001$.

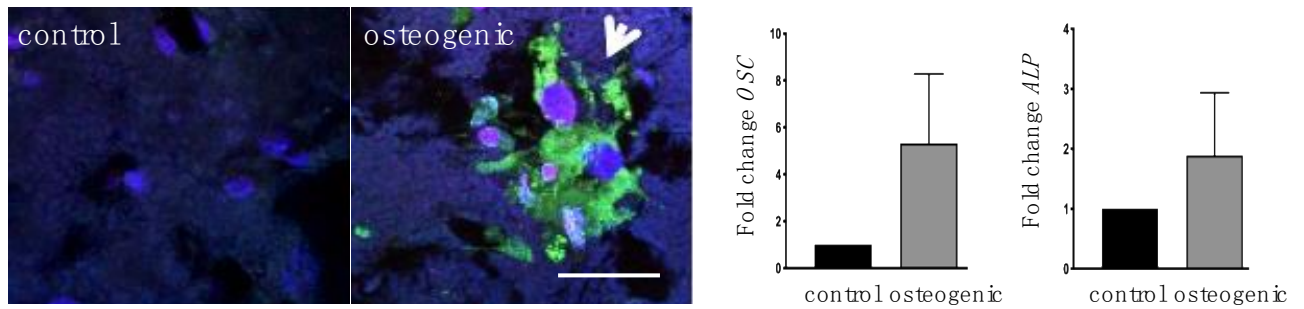


Figure S6. Protein and gene expression after 3 weeks of hADSC osteogenic differentiation on coagulated POSS-PCL. **a)** Immunostaining for Collagen 1 (green) and osteocalcin (red) in control and osteogenically differentiated hADSC. Nuclei are counterstained with Hoechst dye (blue). Scale bar = 100 μm . **b)** Expression of osteocalcin (*OSC*) and alkaline phosphatase (*ALP*) mRNA assessed by RT-qPCR in hADSCs cultured either in control or osteogenic differentiation medium. Data are expressed as mean \pm SEM.

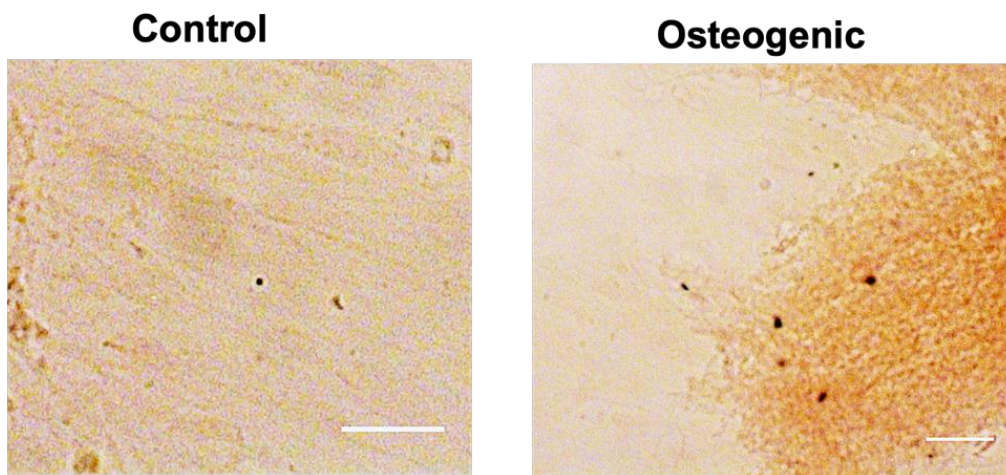


Figure S7. Alizarin red staining hADSC seeded on cast POSS-PCL. Staining is observed following 3 weeks of osteogenic differentiation. It is not possible to stain with alizarin red hADSC differentiated on coagulated POSS-PCL because of extensive trapping/absorption of the dye.

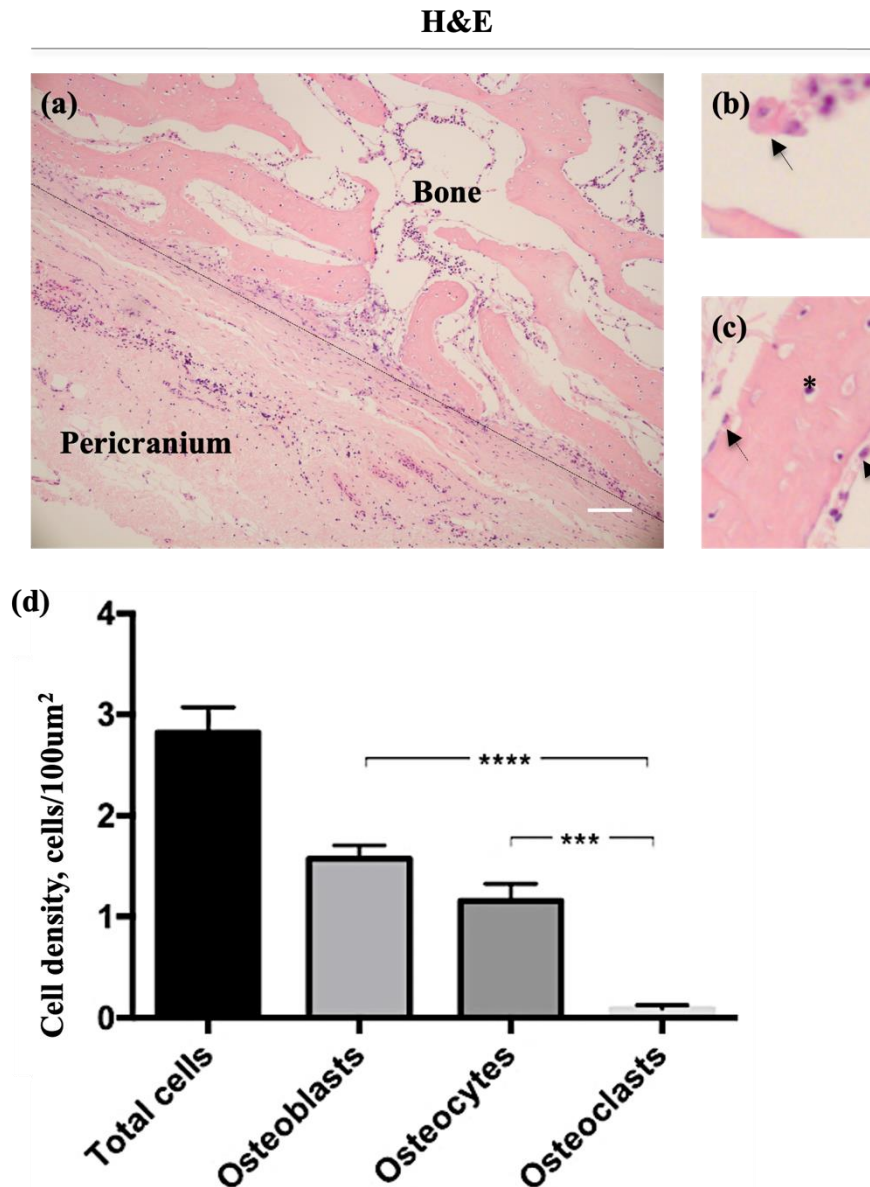


Figure S8. Analysis of native pediatric cranial bone. **a)** Representative section of bone and attached pericranium. The dotted line demarcates exclusion zone for analysis. **b)** Large irregular shaped cells identified as osteoclasts. **c)** Osteoblasts appeared small and cuboidal (arrow) whilst osteocytes were located within the bone mass (*). **d)** Cells counted on H&E sections from different patients ($n = 7$) with average $2.82 (\pm 0.25)$ cells per μm^2 of bone tissue. There is no significant difference between osteoblast (1.57 ± 1.28) and osteocyte (1.16 ± 0.17) density ($p = 0.34$). Osteoclast density (0.088 ± 0.04) is significantly less than that of osteoblasts ($p < 0.0001$) and osteocytes ($p = 0.0003$). Data expressed as mean number of cells/ μm^2 area of tissue \pm SEM; Scale bars = 100 μm ; *** $p < 0.001$; **** $p < 0.0001$.